

Fibonacci anyons and charge density order in the 12/5 and 13/5 plateaus

Roger S. K. Mong,^{1,2} Michael P. Zaletel,³ Frank Pollmann,⁴ and Zlatko Papić⁵

¹*Department of Physics and Astronomy, University of Pittsburgh, Pittsburgh, Pennsylvania 15260, USA*

²*Walter Burke Institute for Theoretical Physics and Institute for Quantum Information and Matter, California Institute of Technology, Pasadena, California 91125 USA*

³*Station Q, Microsoft Research, Santa Barbara, California, 93106-6105, USA*

⁴*Max-Planck-Institut für Physik komplexer Systeme, Nöthnitzer Str. 38, 01187 Dresden, Germany*

⁵*School of Physics and Astronomy, University of Leeds, Leeds, LS2 9JT, United Kingdom*

The $\nu = 12/5$ fractional quantum Hall plateau observed in GaAs wells is a suspect in the search for non-Abelian Fibonacci anyons. Using the infinite density matrix renormalization group, we find clear evidence that—in the absence of Landau level mixing—fillings $\nu = 12/5$ and $\nu = 13/5$ are in the $k = 3$ Read-Rezayi phase. The lowest energy charged excitation is a non-Abelian Fibonacci anyon which can be trapped by a one-body potential. We point out extremely close energetic competition between the Read-Rezayi phase and a charge-density ordered phase, which suggests that even small particle-hole symmetry breaking perturbations can explain the experimentally observed asymmetry between $\nu = 12/5$ and $13/5$. Reducing the thickness of the quantum well drives a transition from the homogeneous Read-Rezayi phase to the charge-density ordered phase, providing a plausible explanation for the absence of a $\nu = 12/5$ plateau in narrow GaAs wells.

I. INTRODUCTION

The richness of the emergent excitations in many-body systems can belie the simplicity of their underlying Hamiltonian. This sentiment underlies the continued effort to realize quantum materials that exhibit fractionalized non-Abelian quasiparticles. Such phases of matter, apart from their fundamental interest, are the proposed building blocks of quantum computers resilient to decoherence.^{1,2}

While significant progress has been made towards realizing emergent Majorana zero modes in a variety of experimental systems,^{3–8} the number of candidate hosts for Fibonacci anyons – which are in some sense an interacting generalization of Majoranas – remains much more limited. Unlike Majoranas, Fibonacci anyons have “universal” braiding statistics: braiding Fibonacci alone is sufficient to approximate any quantum gate.⁹ Various lattice models have been proposed realizing Fibonacci anyons, but they require complex interactions.^{10–14}

Here we investigate one of the simplest possibilities for realizing Fibonacci anyons: as the emergent low-energy excitations of incompressible states at $\nu = \frac{12}{5}$ and $\nu = \frac{13}{5}$ fractional quantum Hall plateaus in GaAs quantum wells.^{15,16} Experiments by Kumar *et al.*¹⁶ on a symmetrically-doped, 30 nm quantum well sample have observed an incompressible state at $\nu = \frac{12}{5}$ with a gap of about 80 mK, larger than expected from the model of non-interacting composite fermions.¹⁷ Curiously, the $\nu = \frac{13}{5}$ plateau is replaced by a reentrant integer quantum Hall state (RIQH) with quantized Hall conductance $\sigma^{xy} = 3\frac{e^2}{h}$, indicative of broken translation invariance and suggesting the formation of charge density order (CDO).^{18–20} A similar RIQH plateau develops directly proximate to the $\nu = \frac{12}{5}$ plateau, so the approximate particle-hole symmetry relating fillings $\frac{12}{5}$ and $\frac{13}{5}$ is at least weakly broken in the given experimental sample.¹⁶

A theoretical proposal for a novel phase at $\nu = \frac{13}{5}$ and $\frac{12}{5}$ filling was put forward by Read and Rezayi.²¹ They described a class of incompressible phases – the \mathbb{Z}_k “Read-Rezayi”

phases (RR_k) – which occur at filling fractions $\nu = \frac{k}{k+2}$. The Laughlin phase²² ($k = 1$) and Moore-Read phase²³ ($k = 2$) are the simplest entries in the Read-Rezayi sequence. The $k = 3$ member (“ \mathbb{Z}_3 state”) at filling $\nu = \frac{3}{5}$ and its particle-hole conjugate at $\nu = 1 - \frac{3}{5}$, which we call RR₃ and $\overline{\text{RR}}_3$ respectively, involve “pairing” of triplets of particles and support Fibonacci excitations. They are candidates for incompressible plateaus at fillings $\nu = \frac{13}{5}$ and $\nu = \frac{12}{5}$, assuming an inert $\nu = 2$ lowest Landau level and full spin-polarization of the remaining “valence” filling $\tilde{\nu} = \frac{3}{5}, \frac{2}{5}$.

While Read and Rezayi proposed a representative wavefunction for the \mathbb{Z}_3 phase which is the ground state of a Hamiltonian with a 4-body interaction,²¹ it is not clear whether the two-body Coulomb interaction could stabilize such a phase. Refs. 21 and 24 presented some evidence that the ground state of the Coulomb interaction at $\nu = \frac{13}{5}$ is described by the RR₃ phase. These exact diagonalization studies were limited to small systems and based on two assumptions: (1) electron spin is fully polarized; and (2) cyclotron energy is infinite (i.e., absence of Landau level mixing). Taken together one cannot account for the particle-hole asymmetry between $\nu = \frac{12}{5}$ and $\nu = \frac{13}{5}$ observed in experiment. More recently, it was suggested that finite sample width²⁵ pushes the Coulomb ground state deeper into the Read-Rezayi phase.²⁶ Tuning the mass gap in chiral Dirac systems was also found to have a favorable effect on the Read-Rezayi state.²⁷ We note that alternative candidate states have been proposed for $\nu = 12/5$,²⁸ which appear to be energetically competitive in small finite systems.²⁹ Most of these studies, however, rely on wavefunction overlaps to identify the phase, which can be ambiguous since two wavefunctions can have a high overlap yet represent different phases. It is desirable to extend the previous studies to larger systems using an unambiguous criteria for identifying a topological phase which can be reliably extrapolated to the thermodynamic limit.

In this work, we utilize two recent methodological advances to determine the nature of the $\nu = 12/5$ plateau. First, using the infinite density matrix renormalization group

(DMRG),^{30,31} the problem can now be studied on the geometry of an infinitely long cylinder at large circumferences,³² greatly reducing finite-size effects and allowing us to investigate the competition between liquid and CDO phases that is more difficult to study on the sphere or torus.^{33–37} Second, advances in the understanding of quantum entanglement in topological phases allow us to use “entanglement spectroscopy” to extract topological invariants from the ground state wavefunctions,^{32,38–42} providing an unambiguous signature of the $\overline{\text{RR}}_3$ phase.

The principle findings of this work are as follows. We establish that the Coulomb interaction gives rise to the $\overline{\text{RR}}_3$ / RR_3 phase at $\nu = \frac{12}{5}$ and $\nu = \frac{13}{5}$, assuming full spin-polarization and no Landau level mixing (Sec. II). Using a recently developed variant of DMRG for studying the properties of a single anyonic excitation,³² we compute the energies and charge distributions of the anyon excitations (Sec. III). We identify the lowest energy charge excitation with the Fibonacci anyon. We probe the spin polarization and verify that the state does indeed spontaneously spin-polarizes by enlarging the Hilbert space to include both spin species (Sec. IV). We also probe the stability of the Read-Rezayi phase against short-range perturbations (Sec. V), and determine the energy scale favoring $\overline{\text{RR}}_3$ phase over the Abelian hierarchy state. Finally, we study the competition between CDO and $\overline{\text{RR}}_3$ phases. In the absence of Landau-level mixing, we indeed find that the Coulomb Hamiltonian has a competing CDO phase with an energy remarkably close to the $\overline{\text{RR}}_3$ phase, on the order of a few mK per flux. In fact, for sufficiently small well thickness w , the CDO phase has lower energy than the $\overline{\text{RR}}_3$ phase, which may explain the absence of $\nu = \frac{12}{5}$ plateau in narrow wells. This close competition implies that even small perturbations arising from Landau level mixing – which breaks particle-hole symmetry – may tune the system between the RIQH and \mathbb{Z}_3 phases.

II. IDENTIFICATION OF $\nu = 12/5$ AND $13/5$ QUANTUM HALL STATES AS THE $k = 3$ READ-REZAYI PHASE

We begin with the simplest model of fully spin-polarized electrons interacting via the Coulomb potential:⁴³

$$V^{\text{Coulomb}} = \int_{\mathbf{r}, \mathbf{r}'} \frac{e^2}{4\pi\epsilon} \frac{:\rho(\mathbf{r})\rho(\mathbf{r}') :}{|\mathbf{r} - \mathbf{r}'|}, \quad (1)$$

where $\mathbf{r} = (x, y, z)$ is a position vector, with a magnetic field in the z -direction. The electron gas is confined in the z -direction by an infinite square well potential of width w . The Coulomb interaction is projected into the spin-polarized $N = 1$ LL of the lowest subband of the square well.^{25,43} Energies are expressed in units of $E_C = e^2/4\pi\epsilon\ell_B$, where ℓ_B is the magnetic length. For reference, a 5 T magnetic field roughly corresponds to $E_C \sim 120$ K for GaAs samples. Without internal degrees of freedom (spins or LL indices), the $\frac{12}{5}$ and $\frac{13}{5}$ states are related by an exact particle-hole symmetry, so we only present results for $\nu = \frac{12}{5}$.

We use infinite DMRG to study the Coulomb interaction (1) on an infinitely long cylinder of circumference L , where

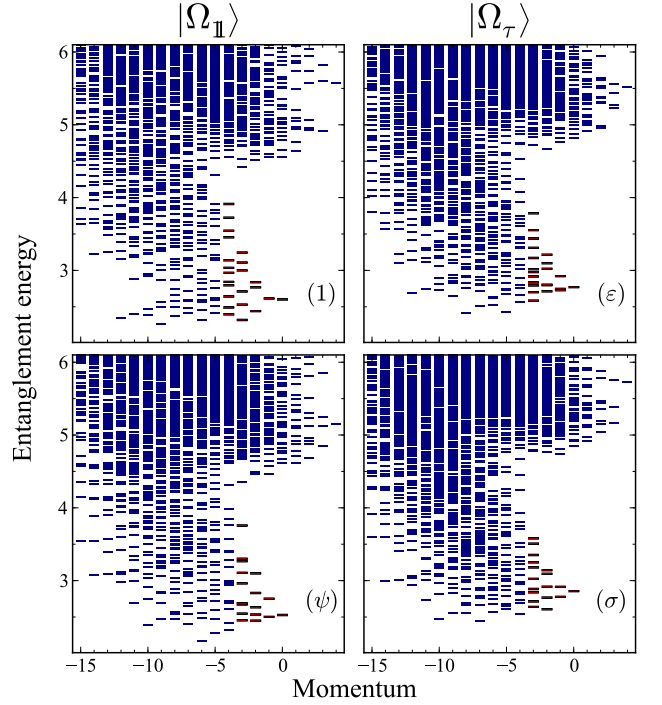


FIG. 1. Orbital entanglement spectra for the two degenerate ground states at $L = 32\ell_B$, $w = 3\ell_B$. For each ground state, we pick two orbital cuts and plot the entanglement energies vs. angular momentum. The low-lying spectra (highlighted in red) agrees with the CFT prediction given in Eq. (2), and thus provides an unambiguous identification of the $\overline{\text{RR}}_3$ phase.

its ground state is expected to have topological degeneracy. Rather than trying to identify the phase via the ground states’ overlap with trial wavefunctions, we examine patterns in the quantum entanglement of the ground states which serve as the “order parameter” for topological order.

For circumferences $L \geq 17\ell_B$, we consistently find ten ground states, as expected for the $\overline{\text{RR}}_3$ phase.⁴⁴ The splitting of the degeneracy is consistent with an exponential decrease with system size, shown in Fig. 2(a). The ten ground states split into two groups of five; within each quintuplet the states are related by translating the center of mass. We label the representative ground states from each quintuplet as $|\Omega_1\rangle$ and $|\Omega_\tau\rangle$.⁴⁵

The first evidence for the $\overline{\text{RR}}_3$ phase comes from the entanglement spectra. We partition the infinite cylinder into left (L) and right (R) halves, each semi-infinitely long. Given a wavefunction $|\Psi\rangle$ on the cylinder, the entanglement spectrum⁴⁶ $\{\epsilon_\alpha\}$ is the set of eigenvalues of $-\log \rho_L$, where $\rho_L = \text{Tr}_R |\Psi\rangle\langle\Psi|$ is the reduced density matrix for the left half of the system. Each eigenvalue ϵ_α is called an “entanglement energy” level, and carries quantum numbers of charge and angular momentum, just as a physical edge of the cylinder would. Generically the low-lying levels of the entanglement spectra (along with their quantum numbers) mimic the physical edge theory of the phase,^{38,46,47} which can be used to identify the topological order. For the $\overline{\text{RR}}_3$ phase, the corresponding edge structure is a product of the \mathbb{Z}_3 parafermion

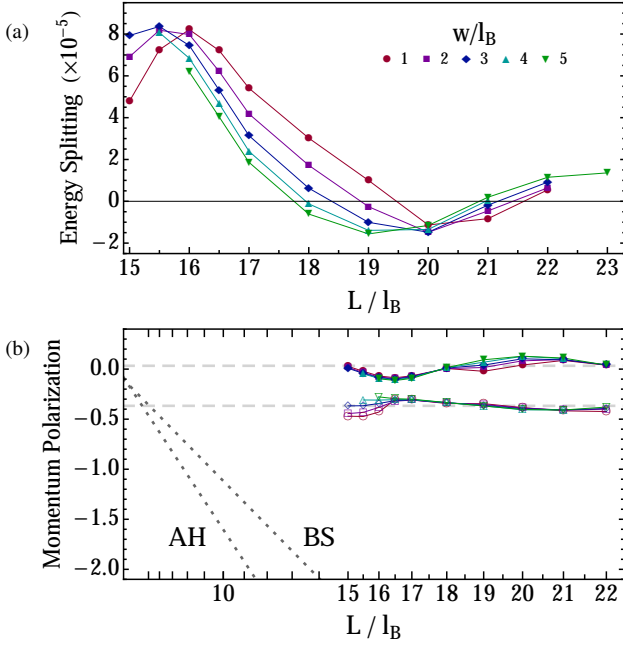


FIG. 2. (a) The splitting of the topological degeneracy $E(|\Omega_\tau\rangle) - E(|\Omega_\mathbb{1}\rangle)$ as a function of cylinder circumference L is consistent with an exponential decrease. w is the width of the well. (b) Scaling of the momentum polarization M with circumference squared L^2 , which reveals the shift \mathcal{S} . Dashed lines indicate the theoretical predictions for the $\mathbb{1}$ and τ ground states of $\overline{\text{RR}}_3$, and dotted lines for the competing hierarchy (AH) and Bonderson-Slingerland (BS) states.

conformal field theory (CFT)⁴⁸ with a $U(1)$ boson. Each entanglement spectra corresponds to one of six primary fields of the \mathbb{Z}_3 parafermion CFT: $1, \psi, \psi^\dagger, \varepsilon, \sigma, \sigma^\dagger$. The predicted level countings (i.e., the number of low-energy states for each momentum) are

$$\begin{aligned} 1 : & 1, 1, 3, 6, 12, \dots, & \varepsilon : & 1, 3, 6, 13, 24, \dots, \\ \psi/\psi^\dagger : & 1, 2, 5, 9, 18, \dots, & \sigma/\sigma^\dagger : & 1, 2, 5, 10, 20, \dots \end{aligned} \quad (2)$$

Figure 1 shows the orbital entanglement spectra for the ground states $|\Omega_{\mathbb{1}/\tau}\rangle$ at $L = 32\ell_B$. The pattern of the low-lying levels (highlighted in the figure) is indicative of a chiral edge mode, with level counting consistent with the corresponding CFT of the Read-Rezayi phase. In each spectra, the first four levels unambiguously match the theoretical prediction.

Robust quantitative evidence for the $\overline{\text{RR}}_3$ state comes from the “momentum polarization”,^{32,42,49} which effectively computes the modular T -transformation. The momentum polarization M is defined to be $M = \text{Tr}[\rho_L \hat{K}]$ with \hat{K} the angular momentum operator on the cylinder; it measures the average amount of momentum carried in the left half of the system. As explained in Ref. 50, M encodes three topological invariants: the “shift”⁵¹ \mathcal{S} , the chiral central charge c , and the anyon topological spin h_a :

$$M[|\Omega_a(L)\rangle] = -\frac{\nu \mathcal{S} L^2}{(4\pi\ell_B)^2} + h_a - \frac{c}{24} + \mathcal{O}(e^{-\frac{L}{\xi}}). \quad (3)$$

Figure 2(b) shows $M(L)$ plot vs. L^2 for ground states $|\Omega_{\mathbb{1}/\tau}\rangle$. From the slope of the data, we see that $\mathcal{S} = 0$, consistent

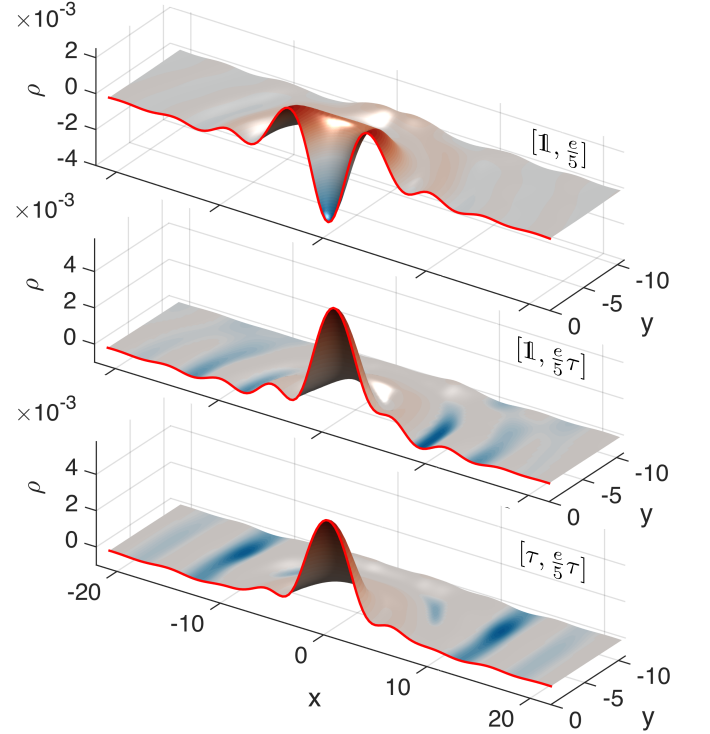


FIG. 3. Cuts through the density profile for anyons with charge $e/5$, computed by using various boundary conditions $[a, b]$ on a $L = 21\ell_B$ cylinder. The pinning potential is a gaussian of width $\approx 4\ell_B$. The top figure shows an Abelian $\frac{e}{5}$ particle while the bottom two shows the Fibonacci $\frac{e}{5}\tau$ anyon. These quasiparticles are about $15\ell_B$ in diameter.

with the $\overline{\text{RR}}_3$ phase and definitively ruling out the $\nu = \frac{2}{5}$ hierarchy phase ($\mathcal{S} = 6$) and the Bonderson-Slingerland (BS) phase ($\mathcal{S} = 4$).^{28,29} The intercepts $h_a - \frac{c}{24}$ are also consistent with $\overline{\text{RR}}_3$ (cf. Appendix A).

III. THE NATURE AND ENERGETICS OF THE ANYONIC EXCITATIONS

Having established the properties of the ground states, we turn our attention to the anyonic excitations. There are a number of anyon properties we can infer from theory – e.g., the anyon types, their charges, and fusion rules. However, we are interested in the non-topological aspect of the anyons relevant to the physical system, which depend on microscopic details. In particular, we wish to study the size, shape, and energetics of the fractional excitations.

There are two anyon types for each charge $m\frac{e}{5}$ ($m \in \mathbb{Z}$), one Abelian and the other of Fibonacci type, which we label $\frac{me}{5}$ and $\frac{me}{5}\tau$ respectively. (For the $m = 0$ neutral particles, we simply label them $\mathbb{1}$ and τ .) The Coulomb interaction will generally drive charges to fractionalize into the smallest possible units, with charge $\pm\frac{e}{5}$, but there remains two possibilities: $\pm\frac{e}{5}$, which are Abelian, and $\pm\frac{e}{5}\tau$, which are non-Abelian. Braiding and fusion of the $\frac{e}{5}\tau$ excitations would in principle be sufficient for universal topological quantum computing.

To answer these questions we perform “defect-DMRG” on an infinite cylinder with the boundary conditions at infinity chosen to trap an anyon at the center of the cylinder.³² The ten degenerate ground states obtained from DMRG are labeled by the topological flux (anyon type) a threading the cylinder, $\{|\Omega_a\rangle\}$. Similar in spirit to the Su-Schrieffer-Heeger soliton of polyacetylene, anyons appear as a “domain wall” between different degenerate ground states in $\{|\Omega_a\rangle\}$, though their energy is point-like, not extensive in the circumference. On the far left / right of the cylinder, we fixed the wavefunction to be $|\Omega_a\rangle / |\Omega_b\rangle$, and variationally optimize the state in a finite portion of the cylinder in order to ‘glue’ these boundary conditions together. (cf. Appendix D) A domain wall of $[a, b]$ (which denotes $|\Omega_a\rangle$ on the left, $|\Omega_b\rangle$ on the right), can trap an anyon of type c if the fusion $a \times c \rightarrow b$ is permitted. In other words, the possible anyon types arising from boundaries $[a, b]$ is the list of possible fusion channels $\bar{a} \times b$, where \bar{a} is the antiparticle of a . The variational procedure will choose the fusion channel with the lowest possible energy.

A domain wall $[1, b]$ will always trap a b -type anyon. In Fig. 3(a) and (b), we show the density distribution of the anyon arising from such boundary conditions, trapping a $\frac{e}{5}$ (Abelian) and $\frac{e}{5}\tau$ (non-Abelian) anyon. Their charge distributions are qualitatively distinct, so in principle they could be distinguished by their quadrupole moment Q_{zz} , where \hat{z} points normal to the plane. For comparison, the sizes of elementary excitations in the model $\overline{\text{RR}}_3$ state are much smaller, $\sim 3\ell_B$ in diameter.⁵² In Fig. 3(c), we set up the domain wall $[\tau, \frac{e}{5}\tau]$, for which there are two possible anyon types allowed by the fusion rules: $\tau \times \frac{e}{5}\tau = \frac{e}{5} + \frac{e}{5}\tau$. The DMRG algorithm should choose the anyon type with lower energy; noting the similarities in the density profile between Fig. 3(b) and (c), it appears the non-Abelian $\frac{e}{5}\tau$ has lower energy than its Abelian counterpart.

To confirm the energetics quantitatively, we define the energy E_a of anyon a to be the energy required to add a to the groundstate in the absence of a pinning potential plus the electrostatic interaction between a charge Q_a point-charge and a neutralizing medium. With this definition, we find $E_{\frac{e}{5}} = -0.0508$ and $E_{\tau\frac{e}{5}} = -0.0511$ at $L = 21\ell_B$, $w = 3\ell_B$.

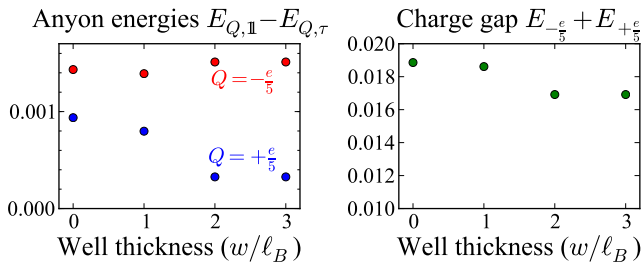


FIG. 4. Anyon excitation energies $E_{Q,a}$ at various quantum well thicknesses, for the $\overline{\text{RR}}_3$ phase in absence of disorder. (Left) The difference between the Abelian and Fibonacci anyons for charges $Q = \pm\frac{e}{5}$. The data shows that for a fixed charge Q , it is energetically favorable to trap a Fibonacci rather than an Abelian anyon. (Right) The energy required to disassociate a pair of $\pm\frac{e}{5}$ quasiparticles. See the main text for caveats in regards to this data.

As expected, the energy of the non-Abelian particle is lower; in addition, the energy $E_{\tau\frac{e}{5}}$ obtained from boundary conditions $[1, \frac{e}{5}\tau]$ is in very good agreement with boundary conditions $[\tau, \frac{e}{5}\tau]$. We find that for well-widths $w = 0-3\ell_B$ and charge $\pm\frac{e}{5}$, the non-Abelian anyon type always has lower energy than the Abelian type. We show this energetic difference (at $L = 21\ell_B$) in Fig. 4. Thus, in the absence of a pinning potential, it is energetically favorable to bind a Fibonacci τ to a $\pm\frac{e}{5}$ charge. Furthermore, when including a pinning potential such as the width $4\ell_B$ Gaussian pin used in Fig. 3, the Fibonacci charge receives a significantly lower potential energy from the pin because its charge distribution is better concentrated at the center. This suggests an array of Fibonacci anyons can be pinned by trapping $\pm\frac{e}{5}$ -charged particles with a weak one-body potential and slowly cooling the system. Such a setup may be employed in a measurement-only quantum computing scheme.⁵³

The “charge gap” for the $\overline{\text{RR}}_3$ phase is the energy required to create and separate a pair of charge $+\frac{e}{5}$, $-\frac{e}{5}$ particles from the ground state, $\Delta = E_{+e/5\tau} + E_{-e/5\tau}$, which we find numerically to be about 0.017. This corresponds to about 2 K at 5 T, far larger than the 80mK activated-transport gap observed in experiments.¹⁶ A similar discrepancy was found for the Moore-Read state at $\nu = \frac{5}{2}$, where numerics find a charge gap of about 0.022 (≈ 2.5 K at 5 T)⁵⁴ while the experiments of Dean *et al.*⁵⁵ report an activated-transport gap of about 0.0047 (≈ 540 mK at 5 T). At $\nu = \frac{5}{2}$ the discrepancy is reduced somewhat by including the effects of Landau-level mixing⁵⁴ and (presumably) dressing the excitation with spin flips, but it is believed that disorder broadening plays a large role as well, for example $\Gamma \approx 0.8$ K in the sample of Dean *et al.*⁵⁶ We cannot say whether the discrepancy at $\nu = 12/5$ could be resolved by including these additional corrections or if qualitatively different physics is involved, such as some signature of the competing CDO discussed below.

IV. EVIDENCE FOR SPONTANEOUS SPIN-POLARIZATION

There have been few experimental studies on the spin-polarization of the $\frac{12}{5}$ plateau.⁵⁷ The experiments of Ref. 57 found that applying an in-plane B -field, which increases the Zeeman splitting, drove the $\frac{12}{5}$ plateau through a transition; at a critical in-plane B -field the gap measured from activated transport closed, then reopened at larger field. A natural explanation, believed to explain similar physics at $\nu = 2/3$,^{58,59} is that the Coulomb point is spin-unpolarized until a critical effective Zeeman field spin-polarizes the phase. Ref. 57 pointed out that the spin transition observed at $\nu = 12/5$ resembles to some extent the transition at $\nu = 2/5$, which likely occurs between the 332 Halperin state⁶⁰ and the Abelian hierarchy (composite fermion) state. In this particular sample, the behavior of the gap of the spin-polarized $\nu = 12/5$ state appeared to conform with the predictions of composite fermion theory¹⁷, although the transport was also anisotropic. It is known, however, that tilt-field experiments are complicated to interpret because the in-plane B field combines with the fi-

nite well width to change the interaction in important ways, for example by mixing in higher sub-bands with a $N = 0$ LL character and reducing the effective well-width.⁶¹

Rather than attempting to model the experiment in Ref. 57, here we are interested in whether the ground state of the Coulomb Hamiltonian (1) spontaneously spin polarizes or not when the Zeeman splitting vanishes. Indeed, the typical Zeeman splitting of the electron spin is small in comparison to the Coulomb energy, $g\mu_B B/E_C \approx \frac{1}{70}$, hence the spin-singlet vs. spin-polarized character of a plateau is largely determined by interactions.

We check the spontaneous spin-polarization of the Coulomb state by keeping the full Hilbert space of both spin species with density $\tilde{\nu} = \frac{1}{5} + \frac{1}{5}$ and enforcing number conservation of each spin separately (we ignore fully filled $\nu = 2$ and Landau level mixing). Using iDMRG, at $w = 3\ell_B$ and $L = 21\ell_B$ we observe long-range ordering of the fermion spin in the XY plane, signaling spontaneous breaking of $SO(3)$ (see Appendix B). Despite the larger Hilbert space, the energy obtained agrees with the spin-polarized filling to good precision. For small system sizes that can be studied by exact diagonalization we also find that the ground state as well as the low-lying energy spectrum are fully spin polarized.

V. STABILITY OF THE READ-REZAYI PHASE AGAINST SHORT-RANGE PERTURBATIONS

The ground state at $\nu = 2/5$ in the $N = 0$ LL is the spin-polarized Abelian hierarchy or composite fermion state, and an obvious competitor at $\nu = 12/5$. Here we examine the stability of the \overline{RR}_3 phase at $\nu = 12/5$ as we perturb the $N = 1$ LL projected Coulomb interaction by the short-range V_1 pseudopotential.

As the node of $N = 1$ LL wavefunctions softens the interaction, we expect that adding $\Delta V_1 > 0$ will drive the \overline{RR}_3 phase back into the Hierarchy phase. This is indeed what happens, Fig. 5. In terms of the ratio V_1/V_3 , the transition between the \overline{RR} and Hierarchy phase is about 1/3 of the way between the Coulomb $N = 1$ and $N = 0$ LLs. ΔV_1 is a ‘best-case’ perturbation for the Hierarchy state, as a typical real-space potential will be distributed across all V_m . In fact, we have verified that projecting a $V(r) = \delta'(r)$ interaction into the $N = 1$ LL favors a CDO phase, not the Hierarchy state. Linearly extrapolating the energy of the Hierarchy state to the Coulomb point, we obtain a splitting between the \overline{RR}_3 and Hierarchy state of about $\Delta E_{H-RR} \sim 1.5 \cdot 10^{-4}$ per flux at well-width $w = 2$.

We directly probe the stability of the entire low-energy spectrum of the \overline{RR}_3 phase upon varying V_1 using exact diagonalization (ED) [Fig. 6]. We assume complete spin polarization and no Landau level mixing. The energy spectrum of the system is resolved as a function of pseudomomentum \mathbf{K} ⁶², and the \overline{RR}_3 phase is characterized by a two-fold degenerate ground state in $\mathbf{K} = 0$ sector. Additionally, as discussed in Sec. II, there are five copies of those that are related by the center of mass translation and can be factored out.

In Fig. 6 we show the phase diagram of the system as V_1

is modified, for zero width (left) and $w/\ell_B = 4$ (right). We compute 10 lowest energies per momentum sector of the system with 25 flux quanta through the hexagonal unit cell. The energies are given in units of E_C , and for clarity we plot them relative to the average energy of the system $\tilde{E} = E - \bar{E}$. Black symbols denote the levels belonging to $\mathbf{K} = 0$ sector. For zero width (left), we identify the \overline{RR}_3 ground state degeneracy in a narrow shaded region around the Coulomb point $\delta V_1 = 0$. In this region the ground state also has large overlap \mathcal{O} with the model \overline{RR}_3 wavefunction (inset). Because of the strong mixing of four lowest energy levels with $\mathbf{K} = 0$ around the Coulomb point, we define the overlap \mathcal{O} as a sum of singular values of the 4×2 overlap matrix $O_{ij} \equiv |\langle \psi_{\text{exact}}^i | \psi_{\overline{RR}_3}^j \rangle|$, $i = 1, \dots, 4$, $j = 1, 2$. At larger width $w/\ell_B = 4$, the \overline{RR}_3 phase widens and becomes more robust as the two quasidegenerate $\mathbf{K} = 0$ levels become better separated from the rest of the spectrum. By inspecting the level degeneracy and computing the overlaps, we also deduce that the \overline{RR}_3 phase is surrounded by the hierarchy/composite fermion state for larger positive δV_1 , and several charge density ordered phases for negative δV_1 . The phase CDO I was identified with a stripe in Ref. 24. The estimate of critical V_1 for the transition into the Hierarchy state is in agreement with DMRG estimate in Fig. 5.

VI. COMPETING CHARGE DENSITY ORDER

In several experiments, the filling $\nu = \frac{13}{5}$ lies within a RIQH plateau (called ‘‘R2c’’) with Hall conductance $\sigma^{xy} = 3\frac{e^2}{h}$,^{18,19} since Galilean invariance implies $\sigma^{xy} = \frac{e^2}{h}\nu$, translation invariance must be strongly broken. It is thought that some form of charge-density order spontaneously develops and is pinned by disorder, neutralizing the fractional filling of electrons/holes in the valence LL. A similar RIQH plateau

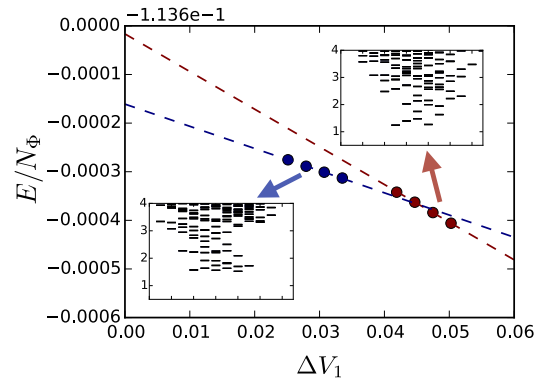


FIG. 5. Transition between the \overline{RR}_3 and Hierarchy states as the Haldane pseudopotential ΔV_1 is added to the Coulomb interaction. In the cylinder geometry the transition is first order. For perspective, in the $N = 0$ LL, $V_1/V_3 = 1.6$; in the $N = 1$ LL, $V_1/V_3 = 1.3$; at the observed transition $V_1/V_3 = 1.43$. Linearly extrapolating the energy of Hierarchy state to the Coulomb point, we obtain a splitting of $\Delta E_{H-RR} \sim 1.5 \cdot 10^{-4}$ per flux. Data is taken from DMRG at $L_x = 20$ and well-width $w = 2$.

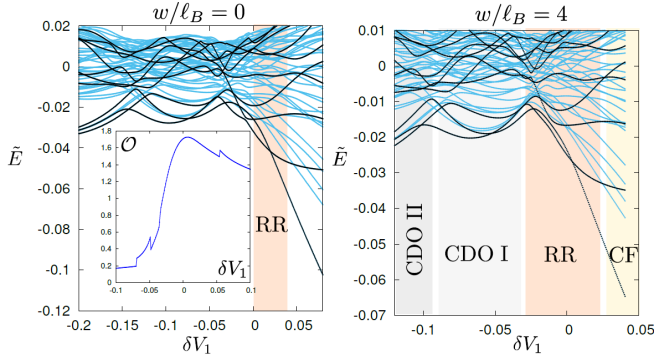


FIG. 6. Phase diagram as a function of modified V_1 pseudopotential, for zero width (left) and $w/\ell_B = 4$ (right). Data is obtained by exact diagonalization of the system with 25 flux quanta through the hexagonal unit cell. We compute the lowest 10 energies (in units of $e^2/\epsilon\ell_B$) per momentum sector and plot them relative to the average energy of the system $\tilde{E} = E - \bar{E}$. Black symbols denote levels in $\mathbf{K} = 0$ sector. For zero width (left), we identify the \mathbb{Z}_3 ground state degeneracy in a narrow shaded region around the Coulomb point $\delta V_1 = 0$. In this region the ground state has large overlap \mathcal{O} with the model \mathbb{Z}_3 wavefunction (inset). At width $w/\ell_B = 4$ (right), the \mathbb{Z}_3 phase widens and becomes more robust. It is surrounded by the hierarchy/composite fermion state for larger positive δV_1 , and several charge density ordered phases for negative δV_1 .

(“R2b”) with $\sigma^{xy} = 2\frac{e^2}{h}$ lies directly proximate to the $\nu = \frac{12}{5}$ plateau. Ref. 19 found that the partial filling at the center of the RIQH plateaus, ν_{2b}, ν_{2c} , very nearly satisfies particle-hole symmetry: $1 - \nu_{2c} = \nu_{2b} - 0.006$. The width of the R2b plateau is a bit thinner than R2c, and $\nu = \frac{12}{5}$ filling just escapes the RIQH region and develops as a separate plateau.¹⁶

The nature of the charge density order in the RIQH R2b and R2c phases is not known.^{18–20,63,64} A Hartree-Fock (HF) analysis predicts that among mean-field states either a two-particle “bubble” (a Wigner crystal of two-electron droplets) or a stripe (smectic) phase may be competitive at $2/5$ and $3/5$ partial filling.^{65–67} For a pure $N = 1$ Coulomb interaction the stripe is predicted to occur at a wavelength $\lambda_{\text{HF}} \approx 4.91\ell_B$.⁶⁷ It is expected that effects beyond HF will spontaneously modulate the density along the stripes, effectively forming an anisotropic bubble phase without the symmetries of the triangular-lattice.^{68,69}

Because our current study neglects LL mixing, our model has a particle-hole symmetry relating valence fillings $\tilde{\nu}, 1 - \tilde{\nu}$, so cannot directly account for the observed asymmetry. Nevertheless the above phenomenology suggests a CDO phase should be in close competition with the $\overline{\text{RR}}_3$ phase, which we show below is the case.

Charge density order is subtle to study in finite-size numerics; the sphere geometry will strongly frustrate CDO while the torus has to be tuned to the correct aspect ratio (this is further discussed in Appendix C). On the infinite cylinder we must consider the finite circumference L and the unit cell used in the infinite DMRG; at filling p/q the unit cell must contain $m \cdot q$ flux ($m \in \mathbb{Z}$), corresponding to a period $\lambda_m = m \cdot q \frac{2\pi\ell_B^2}{L}$ along the length of the cylinder. The $\overline{\text{RR}}_3$ phase is com-

surate with $m = 1$ for all L .

In the numerics presented so far, CDO was implicitly forbidden because we used the minimal DMRG unit cell $m = 1$. To remedy this, we run simulations for a variety of circumferences L and unit cells $m \cdot q$ chosen to accommodate the bubble and stripe phases, even including pinning potentials to preference various orders in the initial stages of the DMRG. For Coulomb interaction plus well width, the only CDO found is a stripe phase with a wavelength λ_{CDO} quite close to λ_{HF} . Even though our geometry is quasi-1D, spontaneously breaking translation is not forbidden by Mermin-Wagner because the magnetic algebra renders the symmetry discrete along the length of the cylinder.

Holding fixed the DMRG unit cell at $m \cdot q$, the wavelength of the CDO is forced to be $\lambda_m = 5m \frac{2\pi\ell_B^2}{L}$. As the circumference L is changed, λ_m deviates from the optimal λ_{CDO} and the CDO is forced to compress or stretch. Consequently we expect the energy density of the CDO depends parabolically on L , via $E \sim (\lambda_m - \lambda_{\text{CDO}})^2$, as found in Fig. 7(a). At $w = 0$, this feature is found both for $m = 3, L \sim 20\ell_B$ and $m = 4, L \sim 27\ell_B$. The optimal λ_{CDO} can be determined from the minimum of the parabola, and depends on w at the level of 10%, with larger w preferring smaller λ_{CDO} .

As shown in Fig. 7(c), the CDO has remarkably close energy ($\Delta E/\text{flux} \sim 10^{-5}$) to the $\overline{\text{RR}}_3$ phase; for $L \sim 20\ell_B$ and $w = 0$, the CDO is the true ground state! Increasing w favors the $\overline{\text{RR}}_3$ state; our finite size numerics points to a transition around $w \sim 1\ell_B$.

While $\lambda_{\text{CDO}} \sim 4.75\ell_B$ is rather close to λ_{HF} , the CDO we find is a highly entangled state rather different from the naive HF ansatz. In the HF ansatz of a stripe, the orbital occupation alternates between $\nu = 1$ and $\nu = 0$, effectively forming decoupled stripes of IQH. Because the IQH has chiral edge modes, the correlations are algebraic along the length of the stripe. As shown in Fig. 7(b), the CDO orbital occupation forms a near perfect sine-wave, with higher Fourier components falling off exponentially in k . This implies that the Greens function decays exponentially along the length of the stripes, suggesting interaction effects have gapped out the chiral edge modes. This appears to be consistent with theoretical predictions that the HF smectic order is unstable towards bubble formation along the stripes.^{68,69} The precise nature of the CDO will have important experimental signatures, and will be investigated in a subsequent work.

VII. SUMMARY AND DISCUSSION

We numerically simulated the fractional quantum Hall effect at a filling factor $\nu = 12/5$ using the infinite density matrix renormalization group and exact diagonalization methods. Our simulations include realistic Coulomb interaction appropriate for GaAs quantum wells of finite width. In the absence of Landau level mixing, the topological properties of the $\nu = 12/5$ ground state are consistent with the $k = 3$ Read-Rezayi phase. The ground state remains spin-polarized for a range of well-widths, even as the Zeeman splitting vanishes. The lowest energy (spin-polarized) charged excitation

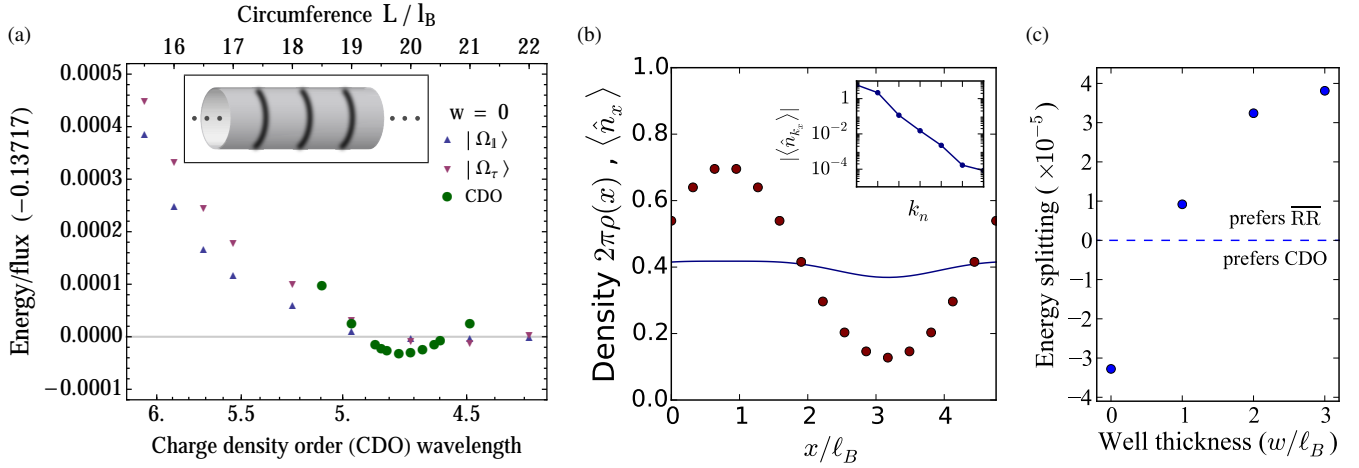


FIG. 7. (a) Energies for the \overline{RR}_3 states (red and blue triangles) as a function of L and CDO (green circles) as a function of wavelength λ , at with zero well-width. For data points denoted by triangles, the energies are computed while enforcing translational invariance of the wavefunctions. The two ground states $|\Omega_{1/\tau}\rangle$ are metastable, and their energy approaches $E_{RR} \approx -0.13717e^2/\ell_B$ in the thermodynamic limit. For data points denoted by circles, a charge density wave of wavelength λ is imposed along the length of the cylinder (illustrated in the inset). Here the CDO minimum E_{CDO} dips below E_{RR} , which suggests that at $w = 0$, the quantum Hall phase is unstable to formation of CDO. (b) Orbital (dots) and real-space (line) density profile of the CDO minima at $\lambda \approx 4.8\ell_B$. Inset shows the Fourier transform of the orbital density, with an exponential decay. (c) Energy splitting (per flux) between the \overline{RR}_3 phase and the CDO phase ($E_{CDO} - E_{RR}$), as a function of w . The data shows that increased well-width w tends to stabilize the Read-Rezayi phase.

was identified with a non-Abelian Fibonacci anyon, which supports universal braid statistics.

The full spin polarization of the ground state and the large charge gap we obtain ($0.017 \sim 2$ K) are encouraging but not in complete agreement with experiments.^{16,57} The estimated gap in Ref. 16 is ~ 80 mK, and Ref. 57 detected a spin transition upon tilting the field. While it may be possible that the lowest charge excitation is actually a skyrmion and/or strongly renormalized by the LL mixing, a better theoretical understanding of activated transport and spin polarization in the exotic 2nd LL plateaus is also desired. As discussed in Ref. 56 in the context of $\nu = 5/2$ plateau, the size of the quasiparticles ($d \sim 15\ell_B$) is comparable to the length scale of disorder arising from the remote ionized donors. In this regime there is a larger tunneling amplitude across saddle points of the disorder potential; it would be interesting if these amplitudes could be numerically estimated using the single-anyon DMRG.

Perhaps most intriguingly, we find an exceptionally close competition between the CDO and \overline{RR}_3 phase. Our numerics shows that with increased width w the \overline{RR}_3 phase is preferred over the CDO; it is advantageous to fabricate the quantum well as wide as possible to stabilize the \overline{RR}_3 phase. At the same time, with increased w the 1st excited subband LL also comes down in energy, crossing with the $N = 1$ LL at $w \sim 3.8\ell_B$. Furthermore, our result suggests that including the perturbative effects of Landau level mixing might explain the asymmetry between the $\nu = \frac{12}{5}$ and $\frac{13}{5}$ plateaus, which would give confidence to the numerics and shed light on the RIQH phases. DMRG can be used to simulate several Landau levels,⁵⁰ so we plan to investigate this possibility in a subsequent study.

Note: During the final preparation of this work, we learned of overlapping results by W. Zhu, D. Haldane and D. Sheng.

ACKNOWLEDGMENTS

RM acknowledges funding from the Sherman Fairchild Foundation. ZP acknowledges support by DOE grant DE-SC0002140. MZ and RM acknowledge support from the visitors program of MPI-PKS Dresden. MZ would like to thank X. L. Qi for time at Stanford University and conversations with C. Nayak and P. Bonderson. We thank Ed Rezayi for advice and collaboration on past studies.

Appendix A: Further characterization of the Read-Rezayi phase via entanglement

We discuss in details the various entanglement measures to identify the $\overline{\text{RR}}_3$ phase at filling $\nu = \frac{12}{5}$. The data presented here are computed assuming full spin-polarization and no Landau level mixing, i.e., a single $n = 1$ Landau level at $\frac{2}{5}$ filling. (The data at $w = 0$ are taken while enforcing a uniform density to stabilize the $\overline{\text{RR}}_3$ phase. It appears rather “messy”, possibly due to a CDO instability.)

We first return to the momentum polarization for the ground states $|\Omega_{\parallel}\rangle$ and $|\Omega_{\tau}\rangle$. As alluded to in the Sec. II, the momentum polarization reveals the shift, chiral central charge c , and topological spin h_a . We numerically calculate the Berry phase $U_{T;a}$ of performing a 2π twist on the left half of the cylinder for ground state $|\Omega_a\rangle$: comparing to the theoretical prediction³²

$$U_{T;a} = \exp \left[2\pi i \left(h_a - \frac{c}{24} - \frac{\eta_H}{2\pi\hbar} L^2 \right) + \dots \right]. \quad (\text{A1})$$

The ellipsis denotes term exponentially suppressed with circumference L , and η_H is the “Hall viscosity”,⁷⁰ related to the shift via $\eta_H = \frac{\hbar}{4} \frac{\nu}{2\pi\ell_B^2} \mathcal{S}$. (For the $\overline{\text{RR}}_3$ phase, the shift is computed at $\nu = \frac{2}{5}$.) The formula given in the main text is the “logarithm” of Eq. (A1), and in principle ambiguous modulo 1. In practice, because $U_{T;a}$ is a continuous function of the circumference, one can easily extract the \mathcal{S} by taking the slope and compute the combination $h - \frac{c}{24}$ modulo 1.

Figure 8(a) shows the momentum polarization for $L = 15\text{--}22\ell_B$, using various range of thicknesses w . From the slope of the data, we extract $\mathcal{S} = 0 \pm 0.1$, in excellent agreement with the $\overline{\text{RR}}_3$ phase at zero shift. Assuming the shift is exactly zero, the data shows the residue $h_a - \frac{c}{24}$. These values corroborate well with those of the $\overline{\text{RR}}_3$ phase with $h_{\parallel} = 0$, $h_{\tau} = -\frac{2}{5}$ and chiral central charge $c = 1 - \frac{9}{5} = -\frac{4}{5}$, shown as the pair of dashed lines.

Finally, we also study the entanglement entropy of the ground states, given by $S = \text{Tr}[-\rho_L \log \rho_L]$. The entanglement entropy is expected to scale with the circumference as $S_a \approx sL - \gamma_a$, where γ_a is a constant called the “topological entanglement entropy” (TEE) associated with anyon type a .^{38,39} The TEE is given by $\gamma_a = \log \mathcal{D} - \log(d_a)$, where d_a are the quantum dimensions of the anyon type a , and \mathcal{D} is the total quantum dimension of the system given by $\mathcal{D}^2 = \sum_a d_a^2$. Figure 8 shows the entanglement entropy as a function of L . Unfortunately the data $S_{\parallel/\tau}$ suffer from very strong finite size effects, it is not possible to extract $\gamma_{\parallel/\tau}$ with any meaningful degree of certainty (the slope s is sensitive to microscopic details and non-universal). However, the difference $S_{\tau} - S_{\parallel} = \gamma_{\parallel} - \gamma_{\tau}$ is universal, predicted to be $\log(\varphi)$ where $\varphi = \frac{1+\sqrt{5}}{2}$ is the golden ratio. While the entropy data alone cannot confirm the existence of a Fibonacci anyon, it is nevertheless completely consistent with the $\overline{\text{RR}}_3$ phase.

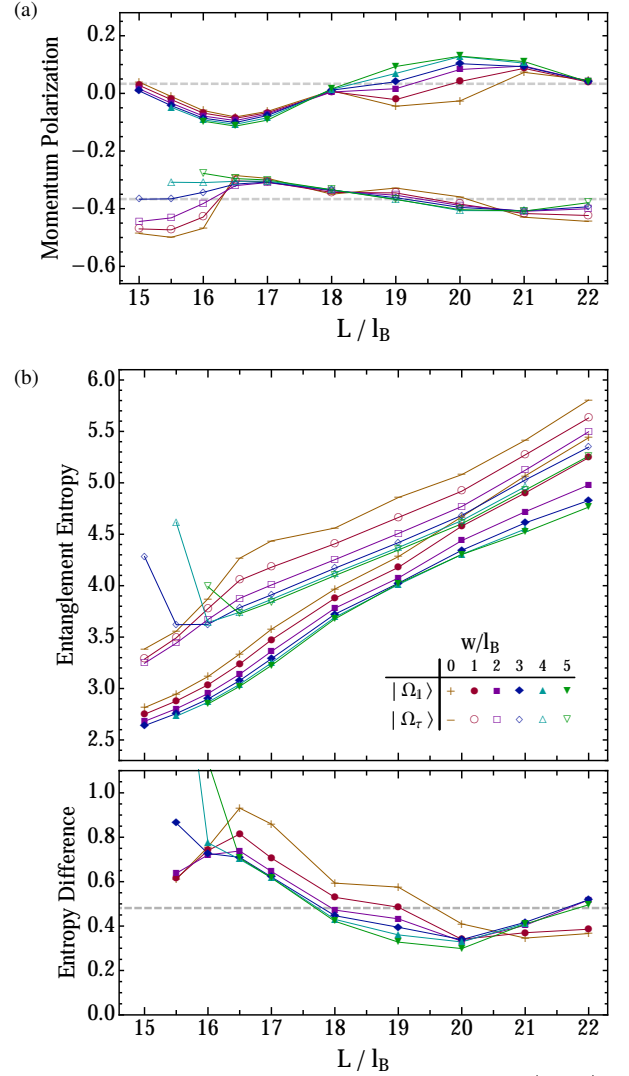


FIG. 8. (a) Momentum polarization for the ground states $|\Omega_{\parallel/\tau}\rangle$. The dashed lines are the predicted values of $h_a - \frac{c}{24}$ for the two ground states. (b) Entanglement entropies S_{\parallel} and S_{τ} , along with their difference $S_{\tau} - S_{\parallel}$. The dashed line at $\log(\varphi) \approx 0.48$ is predicted for the $\overline{\text{RR}}_3$ phase.

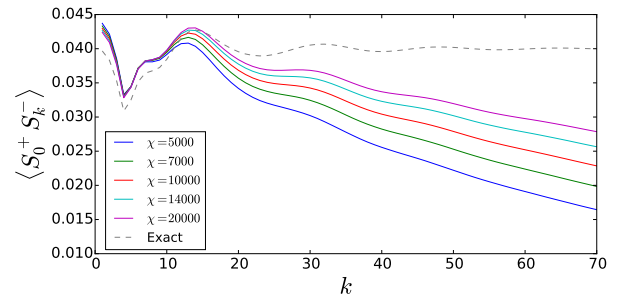


FIG. 9. Spin correlator $\langle S_0^+ S_k^- \rangle$ for $L = 21\ell_B$, $w = 3\ell_B$ at filling $\nu^{\uparrow} = \nu^{\downarrow} = \frac{1}{5}$. Solid curves shows the data at various bond dimensions χ , converging to the expected correlator given as the dashed curve. This is a signature of spontaneously broken spin-rotational symmetry, indicative of a fully spin-polarized ground state at $\nu = \frac{12}{5}$.

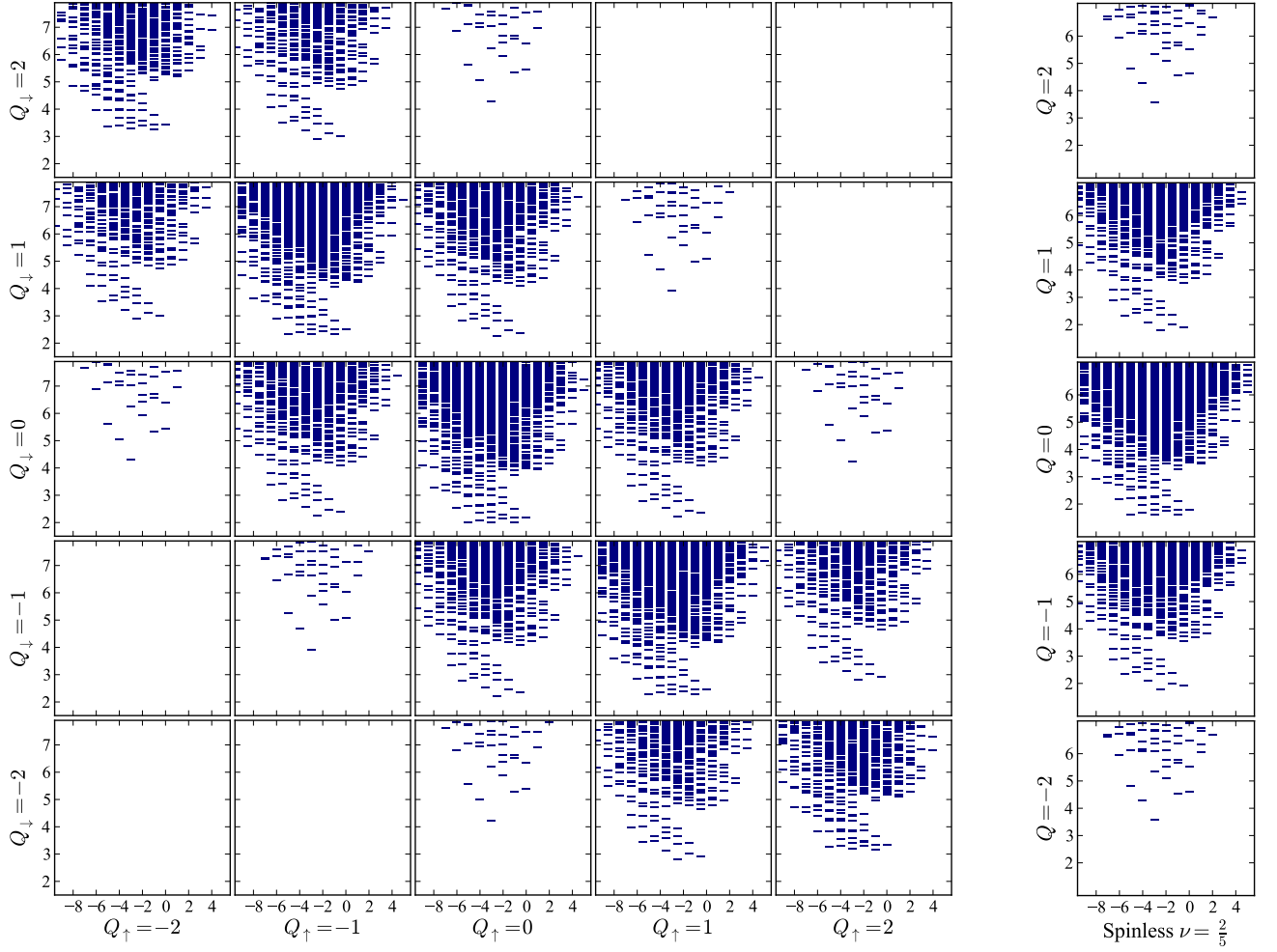


FIG. 10. (Left) The entanglement spectrum of the spin-full system at $\nu^{\uparrow/\downarrow} = \frac{1}{5}$, sorted by charge sector $(Q^{\uparrow}, Q^{\downarrow})$. (Right) The entanglement spectrum for a spinless $\nu = \frac{2}{5}$ system for comparison. Both spectra are taken at $L = 21\ell_B$, $w = 3\ell_B$.

Appendix B: Spin Polarization

We first clarify the expected signatures of spin-polarization when explicitly preserving S^z invariance at filling $\nu^{\uparrow/\downarrow} = \frac{1}{5}$. If $|\theta\rangle_{\overline{\text{RR}}_3}$ represents a $\overline{\text{RR}}_3$ state spontaneously polarized in the XY plane at angle θ , we force the state into the superposition

$$|\Psi\rangle = \int d\theta |\theta\rangle_{\overline{\text{RR}}_3}. \quad (\text{B1})$$

This state has infinite bipartite entanglement, so cannot be represented by a MPS. However, as a variational method the DMRG will do its best, so we expect that the $\langle S^+(r)S^-(r') \rangle$ correlations will be large and nearly constant out to a distance which will depend on the MPS bond-dimension χ , after which it will decay exponentially. (We define $S^+ = c_{\uparrow}^{\dagger}c_{\downarrow}$, and S^- to be its Hermitian conjugate.) This effect (in orbital space) is shown for in Fig. 9 for $L = 21\ell_B$, $w = 3\ell_B$. In the $\chi \rightarrow \infty$ limit, we expect the correlation function to approach the number-number correlator for the $\overline{\text{RR}}_3$ phase (shown in dashed line).

The entanglement spectrum provides further evidence. Recall that the entanglement spectrum can be sorted by the U(1) charges $(Q^{\uparrow}, Q^{\downarrow})$. In Fig. 10 we show the entanglement spectrum for a 5×5 grid of $(Q^{\uparrow}, Q^{\downarrow})$ sectors. For constant Q , the line $Q^{\uparrow} + Q^{\downarrow} = Q$ contains many copies of the charge Q $\overline{\text{RR}}_3$ spectrum, up to some cutoff $|Q^{\uparrow} - Q^{\downarrow}| < S_z^{\text{max}}(\chi)$ that depends on χ . This is because in order to support long-range XY correlations, there must be very large fluctuations in S^z across any bipartition of the system. The entanglement spectrum of a symmetry broken phase was discussed in Ref. 71, where it was shown that the spectrum contain a “tower of states” associated with the broken symmetry; the many identical copies of $\overline{\text{RR}}_3$ we find is this tower of states.

We also note that similar computation was performed for $\nu = \frac{13}{5}$ and we also found evidence for spontaneous spin-polarization.

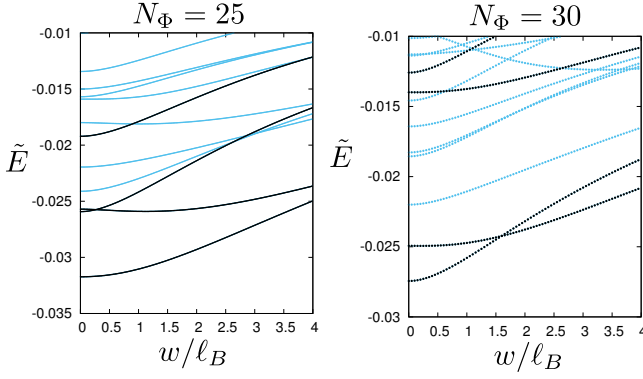


FIG. 11. The effect of finite width w/ℓ_B on the hexagonal torus threaded by $N_\Phi = 25$ flux quanta (left) and $N_\Phi = 30$ (right). Energy spectrum is obtained by exact diagonalization and plotted relative to the average energy of the system. Black symbols denote levels belonging to $\mathbf{K} = 0$ sector.

Appendix C: Exact diagonalization: effects of finite well-width and torus aspect ratio

We showed in Sec. II and VI that finite width stabilizes the homogeneous fluid phase. In Fig. 11(left) we systematically study the effect of well width on the energy spectrum (in particular, the topological ground state degeneracy) via exact diagonalization. We consider a hexagonal torus threaded by $N_\Phi = 25$ and $N_\Phi = 30$ flux quanta.

For a smaller system ($N_\Phi = 25$), the topological degeneracy is not well-resolved for zero width due to the mixing with a higher level belonging to $\mathbf{K} = 0$ sector (black symbols). In this case, the main effect of non-zero w/ℓ_B is to lift the spurious level in energy, leaving a robust two-fold degenerate manifold of ground states. The gap separating these two quasidegenerate states from the rest of the spectrum further widens as w/ℓ_B is increased. At the same time, the overlap with the model Read-Rezayi state slightly increases as a function of width (not shown). For a larger system ($N_\Phi = 30$), the two-fold degeneracy appears to be present already for zero width, but it gets better resolved for moderate widths $w/\ell_B \approx 1.7$.

In Fig. 12(top) we show the effect of changing the geometry of the torus unit cell. We consider a rectangular $L_x \times L_y$ torus in this case, whose area is fixed due by the condition $L_x L_y = 2\pi\ell_B^2 N_\Phi$. By changing one of the linear dimensions of the torus (L_x), we can drive a transition between the homogenous phase and the CDO. In Fig. 12, $L_x \approx 11\ell_B$ corresponds to an isotropic torus ($L_x = L_y$) where the ground state is approximately two-fold degenerate and belongs to the Read-Rezayi phase. Beyond $L_x \approx 19\ell_B$, the system evolves towards another, much deeper, energy minimum, which was identified in Sec. VI with the CDO phase. The difference in ordering between the two phases is captured by the pair correlation function $g(\mathbf{r}) = \frac{L_x L_y}{N_e(N_e-1)} \langle \delta(\mathbf{r} - \mathbf{R}_i + \mathbf{R}_j) \rangle$ shown in Fig. 12(bottom). Unfortunately, because the area of the torus must be preserved as we change L_x , this implies that correlations along the y -direction in the ground state of the system at $L_x \approx 19\ell_B$ are artificially truncated because of small

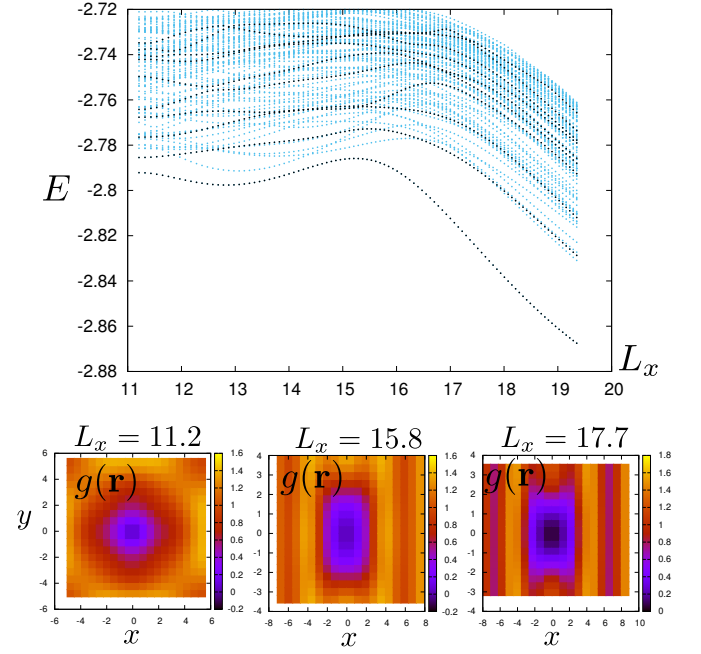


FIG. 12. The effect of changing the geometry (one linear dimension L_x of the torus) on the energy spectrum (top) and the ground state (bottom row) of the system. Energy spectrum is obtained by exact diagonalization of the rectangular torus with $N_\Phi = 20$ flux quanta, and black symbols denote levels belonging to $\mathbf{K} = 0$ sector. Varying L_x induces charge density order in the ground state, as seen in the pair correlation function $g(\mathbf{r})$ for several values of L_x (bottom).

L_y . Therefore, the CDO ground state in this case is likely not faithfully reproduced due to finite-size effects and has significantly less entanglement than what we found by DMRG in Sec. VI.

Appendix D: defect-DMRG

Here we briefly discuss the method use to generate pinned anyons. The iMPS ansatz for a single anyon excitation was discussed in Ref. 32. Because the anyons are charged, in the absence of a pinning potential the single-anyon states form a Landau level. It is convenient to study the anyons in the Landau gauge so that anyon a forms a plane wave with momentum k around the cylinder and is localized near $x \propto k \frac{\ell_B^2}{L}$ along the length. This choice allows us to conserve momentum in the DMRG simulations (interestingly, k is actually fractional because of the topological spin of the anyon). After DMRG we obtain single-anyon states $|k\rangle_a$; just like a Landau level, their energy is independent of k , and different k are related by a magnetic translation T_x along the length of the cylinder. The energy E_a reported in the main text is the energy of $|k\rangle_a$ relative to the ground state, combined with the interaction of a point-charge with a neutralizing background.

We caution that we have not performed finite size scaling of the gaps. If one is familiar with gap calculations on the sphere, this might seem problematic: on a sphere with N electrons,

the corrections are of order $1/N$ and it is imperative to extrapolate gaps in $1/N$. However, the absence of curvature on the cylinder leads to a much more favorable scaling. We can show that if in the thermodynamic limit, the quasiparticle density is bounded by an exponential tail, our estimate of the gap will converge exponentially quickly in the cylinder circumference to its Coulomb value. (Strictly speaking, for a Coulomb interaction the quasiparticles will have $1/r^5$ tails, but this will lead to weak corrections.) For comparison, if we apply the procedure to the integer quantum Hall effect at the same circumference ($L = 21\ell_B$) and precision as the results quoted in the text, we obtain a quasihole energy of $E \approx 1.2531$; the exact result is $\sqrt{\pi}/2 \approx 1.25331$.

To pin the anyons in 2D we need to introduce a pinning potential $\phi(x, y)$, but it is too expensive to work in the full Hilbert space without conserving momentum. In the limit of a weak pinning potential we can use first-order degenerate perturbation theory and project ϕ into the variational space spanned by the anyonic Landau level $\{|k\rangle_a\}$. We compute the many-body matrix elements $H_{kk'}^{\text{eff}} = \langle k' | \hat{\phi} | k \rangle_a$ using standard MPS techniques, diagonalize H^{eff} , and compute the real-space density of the lowest energy state $\sum_k \Psi_k |k\rangle_a$.

The total energy of the pinned excitation is the energy E_a reported in the main text plus the potential energy H^{eff} from the pin. For a width $2\ell_B$ Gaussian, the pin lowers the energy of the non-Abelian $\frac{e}{5}\tau$ excitation by 85% more than the Abelian $\frac{e}{5}$; for a width $6\ell_B$ Gaussian, the difference is 25%.

- ¹ A. Y. Kitaev, Ann. Phys. (NY) **303**, 2 (2003).
- ² C. Nayak, S. H. Simon, A. Stern, M. Freedman, and S. Das Sarma, Rev. Mod. Phys. **80**, 1083 (2008).
- ³ V. Mourik, K. Zuo, S. M. Frolov, S. R. Plissard, E. P. A. M. Bakkers, and L. P. Kouwenhoven, Science **336**, 1003 (2012).
- ⁴ A. Das, Y. Ronen, Y. Most, Y. Oreg, M. Heiblum, and H. Shtrikman, Nat. Phys. **8**, 887 (2012).
- ⁵ L. P. Rokhinson, X. Liu, and J. K. Furdyna, Nat. Phys. **8**, 795 (2012).
- ⁶ M. T. Deng, C. L. Yu, G. Y. Huang, M. Larsson, P. Caroff, and H. Q. Xu, Nano Lett. **12**, 6414 (2012).
- ⁷ A. D. K. Finck, D. J. Van Harlingen, P. K. Mohseni, K. Jung, and X. Li, Phys. Rev. Lett. **110**, 126406 (2013).
- ⁸ H. O. H. Churchill, V. Fatemi, K. Grove-Rasmussen, M. T. Deng, P. Caroff, H. Q. Xu, and C. M. Marcus, Phys. Rev. B **87**, 241401 (2013).
- ⁹ M. H. Freedman, M. J. Larsen, and Z. Wang, Commun. Math. Phys. **227**, 605 (2002).
- ¹⁰ L. Fidkowski, M. Freedman, C. Nayak, K. Walker, and Z. Wang, Commun. Math. Phys. **287**, 805 (2009).
- ¹¹ Z. Liu, E. J. Bergholtz, and E. Kapit, Phys. Rev. B **88**, 205101 (2013).
- ¹² D. Wang, Z. Liu, W.-M. Liu, J. Cao, and H. Fan, Phys. Rev. B **91**, 125138 (2015).
- ¹³ M. Barkeshli, H.-C. Jiang, R. Thomale, and X.-L. Qi, Phys. Rev. Lett. **114**, 026401 (2015).
- ¹⁴ E. M. Stoudenmire, D. J. Clarke, R. S. K. Mong, and J. Alicea, (2015), unpublished, arXiv:1501.05305.
- ¹⁵ J. S. Xia, W. Pan, C. L. Vicente, E. D. Adams, N. S. Sullivan, H. L. Stormer, D. C. Tsui, L. N. Pfeiffer, K. W. Baldwin, and K. W. West, Phys. Rev. Lett. **93**, 176809 (2004).
- ¹⁶ A. Kumar, G. A. Csáthy, M. J. Manfra, L. N. Pfeiffer, and K. W. West, Phys. Rev. Lett. **105**, 246808 (2010).
- ¹⁷ J. K. Jain, *Composite Fermions* (Cambridge University Press, 2007).
- ¹⁸ J. P. Eisenstein, K. B. Cooper, L. N. Pfeiffer, and K. W. West, Phys. Rev. Lett. **88**, 076801 (2002).
- ¹⁹ N. Deng, A. Kumar, M. J. Manfra, L. N. Pfeiffer, K. W. West, and G. A. Csáthy, Phys. Rev. Lett. **108**, 086803 (2012).
- ²⁰ N. Deng, J. D. Watson, L. P. Rokhinson, M. J. Manfra, and G. A. Csáthy, Phys. Rev. B **86**, 201301 (2012).
- ²¹ N. Read and E. Rezayi, Phys. Rev. B **59**, 8084 (1999).
- ²² R. B. Laughlin, Phys. Rev. Lett. **50**, 1395 (1983).
- ²³ G. Moore and N. Read, Nucl. Phys. B **360**, 362 (1991).
- ²⁴ E. H. Rezayi and N. Read, Phys. Rev. B **79**, 075306 (2009).
- ²⁵ M. R. Peterson, T. Jolicœur, and S. Das Sarma, Phys. Rev. B **78**, 155308 (2008).
- ²⁶ Z. Papić, N. Regnault, and S. Das Sarma, Phys. Rev. B **80**, 201303 (2009).
- ²⁷ D. A. Abanin, Z. Papić, Y. Barlas, and R. N. Bhatt, New Journal of Physics **14**, 025009 (2012).
- ²⁸ P. Bonderson and J. K. Slingerland, Phys. Rev. B **78**, 125323 (2008).
- ²⁹ P. Bonderson, A. E. Feiguin, G. Möller, and J. K. Slingerland, Phys. Rev. Lett. **108**, 036806 (2012).
- ³⁰ S. R. White, Phys. Rev. Lett. **69**, 2863 (1992).
- ³¹ I. P. McCulloch, “Infinite size density matrix renormalization group, revisited,” (2008), arXiv:0804.2509.
- ³² M. P. Zaletel, R. S. K. Mong, and F. Pollmann, Phys. Rev. Lett. **110**, 236801 (2013).
- ³³ N. Shibata and D. Yoshioka, Phys. Rev. Lett. **86**, 5755 (2001).
- ³⁴ A. E. Feiguin, E. Rezayi, C. Nayak, and S. Das Sarma, Phys. Rev. Lett. **100**, 166803 (2008).
- ³⁵ D. L. Kovrizhin, Phys. Rev. B **81**, 125130 (2010).
- ³⁶ J. Zhao, D. N. Sheng, and F. D. M. Haldane, Phys. Rev. B **83**, 195135 (2011).
- ³⁷ Z.-X. Hu, Z. Papić, S. Johri, R. Bhatt, and P. Schmitteckert, Physics Letters A **376**, 2157 (2012).
- ³⁸ A. Kitaev and J. Preskill, Phys. Rev. Lett. **96**, 110404 (2006).
- ³⁹ M. Levin and X.-G. Wen, Phys. Rev. Lett. **96**, 110405 (2006).
- ⁴⁰ Y. Zhang, T. Grover, A. Turner, M. Oshikawa, and A. Vishwanath, Phys. Rev. B **85**, 235151 (2012).
- ⁴¹ L. Cincio and G. Vidal, Phys. Rev. Lett. **110**, 067208 (2013).
- ⁴² H.-H. Tu, Y. Zhang, and X.-L. Qi, Phys. Rev. B **88**, 195412 (2013).
- ⁴³ R. E. Prange and S. M. Girvin, *The Quantum Hall Effect* (Springer-Verlag, New York, 1990).
- ⁴⁴ For data in the $\overline{\text{RR}}_3$ phase, we impose translational invariance of the ground state wavefunction to bias against CDO states.
- ⁴⁵ We choose $|\Omega_1\rangle$ to have lower entanglement entropy than that of $|\Omega_7\rangle$.
- ⁴⁶ H. Li and F. Haldane, Phys. Rev. Lett. **101**, 010504 (2008).
- ⁴⁷ X.-L. Qi, H. Katsura, and A. W. W. Ludwig, Phys. Rev. Lett. **108**, 196402 (2012).
- ⁴⁸ A. B. Zamolodchikov and V. Fateev, JETP **62**, 215 (1985), [Zh. Eksp. Teor. Fiz., **89**, 380–399].
- ⁴⁹ Y. Park and F. D. M. Haldane, Phys. Rev. B **90**, 045123 (2014).
- ⁵⁰ M. P. Zaletel, R. S. K. Mong, F. Pollmann, and E. H. Rezayi, Phys.

- Rev. B **91**, 045115 (2015).
- ⁵¹ X. G. Wen and A. Zee, Phys. Rev. Lett. **69**, 953 (1992).
- ⁵² Y.-L. Wu, B. Estienne, N. Regnault, and B. A. Bernevig, Phys. Rev. Lett. **113**, 116801 (2014).
- ⁵³ P. Bonderson, M. Freedman, and C. Nayak, Phys. Rev. Lett. **101**, 010501 (2008).
- ⁵⁴ R. H. Morf, N. d’Ambrumenil, and S. Das Sarma, Phys. Rev. B **66**, 075408 (2002).
- ⁵⁵ C. R. Dean, B. A. Piot, P. Hayden, S. Das Sarma, G. Gervais, L. N. Pfeiffer, and K. W. West, Phys. Rev. Lett. **100**, 146803 (2008).
- ⁵⁶ J. Nuebler, V. Umansky, R. Morf, M. Heiblum, K. von Klitzing, and J. Smet, Phys. Rev. B **81**, 035316 (2010).
- ⁵⁷ C. Zhang, C. Huan, J. S. Xia, N. S. Sullivan, W. Pan, K. W. Baldwin, K. W. West, L. N. Pfeiffer, and D. C. Tsui, Phys. Rev. B **85**, 241302 (2012).
- ⁵⁸ J. P. Eisenstein, H. L. Stormer, L. N. Pfeiffer, and K. W. West, Phys. Rev. B **41**, 7910 (1990).
- ⁵⁹ N. Kumada, D. Terasawa, M. Morino, K. Tagashira, A. Sawada, Z. F. Ezawa, K. Muraki, Y. Hirayama, and T. Saku, Phys. Rev. B **69**, 155319 (2004).
- ⁶⁰ B. I. Halperin, Helv. Phys. Acta. **56**, 75 (1983).
- ⁶¹ Z. Papić, Phys. Rev. B **87**, 245315 (2013).
- ⁶² F. D. M. Haldane, Phys. Rev. Lett. **55**, 2095 (1985).
- ⁶³ F. D. M. Haldane, E. H. Rezayi, and K. Yang, Phys. Rev. Lett. **85**, 5396 (2000).
- ⁶⁴ A. V. Rossokhaty, S. Lüscher, J. A. Folk, J. D. Watson, G. C. Gardner, and M. J. Manfra, “Bias-induced breakdown of electron solids in the second Landau level,” (2014), arXiv:1412.1921.
- ⁶⁵ M. M. Fogler, A. A. Koulakov, and B. I. Shklovskii, Phys. Rev. B **54**, 1853 (1996).
- ⁶⁶ R. Moessner and J. T. Chalker, Phys. Rev. B **54**, 5006 (1996).
- ⁶⁷ M. O. Goerbig, P. Lederer, and C. Morais Smith, Phys. Rev. B **68**, 241302 (2003).
- ⁶⁸ A. H. MacDonald and M. P. A. Fisher, Phys. Rev. B **61**, 5724 (2000).
- ⁶⁹ D. G. Barci, E. Fradkin, S. A. Kivelson, and V. Oganesyan, Phys. Rev. B **65**, 245319 (2002).
- ⁷⁰ J. E. Avron, R. Seiler, and P. G. Zograf, Phys. Rev. Lett. **75**, 697 (1995).
- ⁷¹ M. A. Metlitski and T. Grover, (2011), arXiv:1112.5166.